V European Conference on Computational Fluid Dynamics
ECCOMAS CFD 2010
J. C. F. Pereira and A. Sequeira (Eds)
Lisbon, Portugal, 14–17 June 2010

MATHEMATICAL MODELING OF NON-PERIODIC FLOWS USING FOURIER PSEUDO-SPECTRAL AND IMMERSED BOUNDARY METHODS

Felipe P. Mariano[*], Leonardo Q. Moreira[*], and Aristeu da Silveira Neto[*]

[*] Federal University of Uberlândia - UFU, Faculty of Mechanical Engineering - FEMEC,
Fluid Mechanics Laboratory - MF_{Lab}
Av: João Naves de Avilla, 2121
Campus Santa Mônica, Bl: 5P
Uberlândia, MG, Brasil, CEP: 38400-902
e-mail: {fpmariano, lqmoreira, aristeus}@mecanica.ufu.br

Key words: Fluid Dynamics, Fourier pseudo-spectral method, Immersed boundary method, Green-Taylor flow, Flow over a cylinder.

Abstract. *In the present work it is shown that it is possible to model and simulate non-periodic flows using Fourier Pseudo-Spectral Method (FPSM) coupled with Immersed Boundary Method (IBM) and obtain, at least, second order convergence rates. The IBM has been widely used in Computational Fluids Dynamic (CFD) in order to simulate flows over complex and moving geometries. IBM represents the boundary conditions through a force field added to the Navier-Stokes equations. Nevertheless, generally, it presents low accuracy and low convergence order. On the other hand, the FPSM provides an excellent numerical accuracy and, using the FFT algorithm, it presents a low computational cost compared with other high-order methods. Another important issue, for solving the incompressible Navier-Stokes equations, is the projection method for pressure term, at Fourier space. This procedure does not require a Poisson solver, which is usually the most computational onerous part in classical projection methods. The drawback of FPSM are boundary conditions, which should be periodics, when the Discret Fourier Transform is used. At the present paper, a new method is proposed, which make use of FPSM coupled with IBM, aiming to simulate non-periodic flows over complex geometries. By using a buffer domain and multi-direct forcing method it is possible to represent the boundary conditions and immersed bodies through of force field and obtain high convergence rates and accuracy. In order to validate the new methodology it was proposed the simulations of three problems. The first is a Manufactured Solution problem, which has analytical solution and ability to show accuracy and high order convergence rate (fourth order). The second one is the Poiseuille flow, in which a solid boundary conditions is imposed and second order convergence rate is reached. The last one, assessed is the flow around a circular cylinder, in which quantitative parameters as for instance, drag and lift coefficients and Strouhal number are compared with reference works.*

1 INTRODUCTION

Phenomena involving aeroacustic, transition to turbulence and combustion are problems that modern engineers aim to understand, among other manners, by using techniques of Computational Fluids Dynamics (CFD) [1]. In the case of the aeroacustic problems it is important to use a method that captures the sound pressure waves. In phenomena involving transition to turbulence is necessary to study small instabilities that give rise to turbulence. In combustion, there are processes that involve small edges of turbulent structures. In these problems CFD uses methods of high order accuracy to obtain results to analyze which really represent the physics phenomena mentioned.

High order methods provide an excellent accuracy, for example, high order finite differences method and compact schemes [2]. On the other hand, they have disadvantaged of computational expensive cost in comparison to conventional methodologies. The advents of spectral methods become possible to joining high accuracy with low computational cost [3-5]. This low cost is given by the Fast Fourier Transform (FFT) [6], since the cost of a problem resolution with finite differences is order of $O(N^2)$, where N is the number of the grid points, the cost of the FFT is of $O(N\log_2 N)$ [4]. In addition, it was also developed the projection method [4], which gives the pressure field in the spectral space. Using the projection process is not necessary to calculate the Poisson equation, as it is has been done by conventional methodologies. Normally, solving this equation is the most expensive part of a CFD codes. The disadvantage of the spectral methodology is the difficulty to work with complex geometries and boundary conditions.

One of the most practical methodologies to work with complex geometries is the Immersed Boundary (IBM) [7]. It is characterized by the imposition of a term source, which has the role of a body force added to the Navier-Stokes equation to represent virtually a body immersed in the flow [8].

A new methodology, presented in this paper, works with Fourier pseudo-spectral method connected with immersed boundary method. It is proposed to simulate flows with non-periodic boundary conditions making use of the term source of immersed boundary. On the other hand, the accuracy of immersed boundary is improved, at least to second order for smooth solution problems.

2 MATHEMATICAL MODELING

The mathematical model presented in this section is based on immersed boundary method and in Multi-Direct Forcing proposed by [9]. The equations that govern the problem will be transformed for the Fourier spectral space using the properties of discrete Fourier transform and, finally, the methodology proposed in the present paper concern these two methodologies.

2.1 Mathematical model for the fluid

The flow is governed by momentum and continuity equations. The information of the fluid/solid interface (domain Γ, see Figure 1) is passed to the eulerian domain (Ω) by the addition of the term source to Navier-Stokes equations, term f at equation (1). This term plays a role of a body force that represents the boundary conditions of the immersed geometry [8]. The equations that govern the problem are presented in the tensorial form:

$$\frac{\partial u_l}{\partial t} + \frac{\partial u_l u_j}{\partial x_j} = -\frac{\partial p}{\partial x_l} + \nu \frac{\partial^2 u_l}{\partial x_j \partial x_j} + f_l \tag{1}$$

$$\frac{\partial u_j}{\partial x_j} = 0 \tag{2}$$

where $\frac{\partial p}{\partial x_l} = \frac{1}{\rho}\frac{\partial p^*}{\partial x_l}$; p^* is the static pressure in [N/m^2]; u_l is the velocity in l direction in [m/s]; $\frac{f_l^*}{\rho}$; f_l^* is the term source in [N/m^3]; ρ is the density; ν is the cinematic viscosity in [m^2/s]; x_l is the spatial component (x,y) in [m] and t is the time in [s]. The initial condition is any velocity field that satisfies the continuity equation.

The source term is defined in all domain Ω, but presents values different from zeros only in the points that coincide with the immersed geometry, enabling that the eulerian field perceives the presence of solid interface [10].

$$f_l\ (\vec{x},t) = \begin{cases} F_l(\vec{x}_k,t) & if\ \ \vec{x} = \vec{x}_k \\ 0 & if\ \ \vec{x} \neq \vec{x}_k \end{cases} \tag{3}$$

where $\vec{x}$ is the position of any particle in the fluid and $\vec{x}_k$ is the position of any point in solid interface (figure 1).

The boundary conditions are periodic in all directions in eulerian domain Ω_B, as showed in figure 1, it is necessary due pseudo-spectral method properties. The boundary condition of the simulated problem is imposed by direct forcing methodology in Γ_{BC}, and also the boundary conditions of bodies immersed in flow Γ_i.

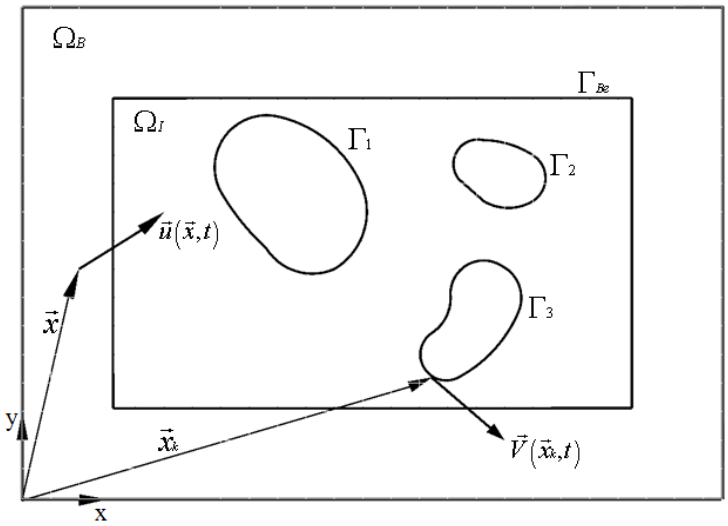

Figure 1: Schematically representation of Eulerian and Lagrangean domain.

Using equation (3) it is possible to concluded that the field $f_l\ (\vec{x},t)$ is discontinuous, which can be numerically solved only when there are coincidence between the Lagragean points with Eulerian domain. In the cases there is no coincidence between these points, which is very frequent in the complex geometries, it is necessary to distribute the function $f_l\ (\vec{x},t)$ on its neighborhoods. Just by calculating the Lagrangean force field $F_l(\vec{x}_k,t)$, it can be distributed and thus, transmitted the geometry presence information for the Eulerian domain. More details about this procedure can be found in [11-12]:

$$\vec{f}(\vec{x}) = \sum_{\Gamma} D_h(\vec{x} - \vec{x}_l)\vec{F}(\vec{x}_l)h^2, \tag{4}$$

$$D_h(\vec{x}_k - \vec{x}) = \frac{1}{h^2} W_c\left(\frac{x_k - x}{h}\right) W_c\left(\frac{y_k - y}{h}\right), \tag{5}$$

$$W_c(r) = \begin{cases} 1 - \frac{1}{2}|r| - |r|^2 + \frac{1}{2}|r|^3 & if\ 0 \le |r| < 1 \\ 1 + \frac{11}{6}|r| + |r|^2 - \frac{1}{6}|r|^3 & if\ 1 \le |r| < 2 \\ 0 & if\ 2 \le |r| \end{cases} \tag{6}$$

Here h is the spacing between two consecutive Lagrangean points.

2.2 Mathematical model for the immersed interface

The Lagrangean force field, in this study, is calculated by direct forcing methodology, which was proposed by [13]. One of the characteristics of this model is that is not necessary to use ad-hoc constants and allows the non-slip condition modeling on immersed interface. The Lagrangean force $F_l(\vec{x}_k, t)$ is available by momentum conservation equation over a fluid particle that is joined in the fluid-solid interface:

$$F_l(\vec{x}_k, t) = \frac{\partial u_l}{\partial t}(\vec{x}_k, t) + \frac{\partial}{\partial x_j}\left(u_l u_j\right)(\vec{x}_k, t) + \frac{\partial p}{\partial x_l}(\vec{x}_k, t) - \nu \frac{\partial^2 u_l}{\partial x_j \partial x_j}(\vec{x}_k, t) \tag{7}$$

The values of $u_l(\vec{x}_k, t)$ and $p(\vec{x}_k, t)$ are given by interpolation of velocities and pressure, respectively, of the Eulerian points near the immersed interface [11]. For Lagrangean point $\vec{x}_k$ at the immersed boundary, we have:

$$F_l(\vec{x}_k, t) = \frac{u_l(\vec{x}_k, t + \Delta t) - u_l^*(\vec{x}_k, t + \Delta t) + u_l^*(\vec{x}_k, t + \Delta t) - u_l(\vec{x}_k, t)}{\Delta t} + RHS(\vec{x}_k, t), \tag{8}$$

where u^* is a temporary parameter, as defined by [9], Δt is the time step and $RHS(\vec{x}_k, t) = \frac{\partial}{\partial x_j}\left(u_l u_j\right)(\vec{x}_k, t) + \frac{\partial p}{\partial x_l}(\vec{x}_k, t) - \nu \frac{\partial^2 u_l}{\partial x_j \partial x_j}(\vec{x}_k, t)$. The equation (8) is solved by equations (9) and (10) at same time step:

$$\frac{u_l^*(\vec{x}_k, t + \Delta t) - u_l(\vec{x}_k, t)}{\Delta t} + RHS(\vec{x}_k, t) = 0, \tag{9}$$

$$F_l(\vec{x}_k, t) = \frac{u_l(\vec{x}_k, t + \Delta t) - u_l^*(\vec{x}_k, t + \Delta t)}{\Delta t}, \tag{10}$$

where $u_l(\vec{x}_k, t + \Delta t) = U_{FI}$ is the immersed boundary velocity, normally known.

Equation (9) is solved at Eulerian domain at Fourier spectral space, *i.e.* the solution of equation (1) with $f_l = 0$. $u_l^*(\vec{x}, t + \Delta t)$ is interpolated for Lagrangean domain and became $u_l^*(\vec{x}_k, t + \Delta t)$ and it is computed on equation (10). Then $F_l(\vec{x}_k, t)$ is smeared for Eulerian mesh by equation (4). Finally, the Eulerian velocity is update by equation (11):

$$u_l\left(\vec{x},t+\Delta t\right)=u_l^*\left(\vec{x},t+\Delta t\right)+\Delta t\cdot f_l\left(\vec{x},t\right) \tag{11}$$

2.3 Fourier Transforms

Defined the equations that govern the flow through immersed boundary method, the next step is transforming them to the Fourier spectral space. Appling the Fourier transform in the continuity, equation (2):

$$ik_j\hat{u}_j=0. \tag{12}$$

According to analytic geometry the scalar product between two vectors is null, if both are just orthogonal. Therefore, from equation (12), the wave number vector k_j is orthogonal to transformed velocity $\hat{u}_j$. The plane of divergent free, here named plane π, is perpendicular to wave number vector $\vec{k}$ and thus, transformed velocity vector $\hat{u}_j\left(\vec{k},t\right)$ belongs to the plane π. Now applying the Fourier transform in the momentum equation (9):

$$\frac{\partial\hat{u}_l^*}{\partial t}+ik_j\widehat{u_l^*u_j^*}=-ik_l\hat{p}-\nu k^2\hat{u}_l^*, \tag{13}$$

where k^2 is the square norm of wave number vector, *i.e.* $k^2=k_jk_j$.

In agreement with plane π definition, each of the terms of equation (13) assume a position related to it: the transient term, $\frac{\partial\hat{u}_l^*}{\partial t}$, and the viscous term, $\nu k^2\hat{u}_l^*$, belong to the plane π. The gradient pressure term is perpendicular to plane π, and non-linear term, $ik_j\widehat{u_l^*u_j^*}$, a priori, is not known in which position it can be found as relation to plane π.

By joining the terms of equation (13) and observing the definition of plane π, we have found that:

$$\underbrace{\left[\frac{\partial\hat{u}_l^*}{\partial t}+\nu k^2\hat{u}_l^*\right]}_{\in\pi}+\underbrace{\left[ik_j\widehat{u_l^*u_j^*}+ik_l\hat{p}\right]}_{\Rightarrow\in\pi}=0, \tag{14}$$

To close equation (14) the addition of pressure and non-linear term must be equal to the projection of the non-linear term over the plane π. For that, a projection tensor is used as in [3], which projects any vector over the plane π. Therefore, applying this definition on the right hand side of the sum done in equation (14):

$$\left[ik_j\widehat{u_l^*u_j^*}+ik_l\hat{p}\right]=\wp_{lm}\left[ik_j\widehat{u_m^*u_l^*}\right]. \tag{15}$$

The parcel of the gradient pressure field is orthogonal to plane π, then, it is zero after to be projected. Therefore we do not need the pressure field to solve Navier-Stokes equations in the spectral space. The pressure field can be recovered at the pos-processing manipulating equation (15).

Other important point is that the non-linear term, in which the product of transformed functions appears, in agreement with Fourier transformed properties, this operation is a convolution product and its solution is given by convolution integral, which is very hard to be performed. This is solved by pseudo-spectral Fourier method [4]. Therefore the momentum equation in the Fourier space, using the projection method, assumes the following form:

$$\frac{\partial \hat{u}_l^*\left(\vec{k},t\right)}{\partial t}+\nu k^2\hat{u}_l^*\left(\vec{k},t\right)=-ik_j\wp_{lm}\int_{\vec{k}=\vec{r}+\vec{s}}\hat{u}_m^*\left(\vec{r},t\right)\hat{u}_l^*\left(\vec{k}-\vec{r},t\right)d\vec{r} \tag{16}$$

The non-linear term can be handed by different forms: advective, divergent, skew-symmetric or rotational [3]. In spite of being mathematically the same, they present different properties when discretized. The skew-symmetric form is more stable and present best results, but it is twice more expensive than the rotational form. However, this inconvenience can be solved using the alternate skew-symmetric form, which consist in to alternate the advective and divergent forms in each time step. This procedure is adopted in present paper.

For all types of hande the non-linear term it is necessary to solve the convolution integral, but its numerical solution is computational expensive. Then the pseudo-spectral method is used, *i.e.* calculates the velocity product in the physical space and transforms this product to the spectral space.

The Navier-Stokes equations is solved numerically with the Fourier spectral method using the Discrete Fourier Transform (DFT), which is define by [14]:

$$\hat{f}_k=\sum_{n=-N/2+1}^{N/2}f_n e^{\frac{-i2\pi kn}{N}}, \tag{17}$$

where $\vec{k}$ is the wave number, N is number of meshes points, n gives the position x_n of collocation points ($x_n=n\Delta x$) and $i=\sqrt{-1}$.

The DFT restriction is the periodic boundary conditions, by limiting the use of Fourier spectral transformed for CFD problems. The advantage is the low computational cost given by Fast Fourier Transform (FFT) [6], which solves the DFT, equation (17), very efficiently way, given order $O(Nlog_2N)$. For systems with many collocation points, *e.g.* three-dimensional problems, the spectral method is very cheaper when compared with another conventional high order methodologies. Two examples of use of this method are the simulations of periodic temporal jets and isotropic turbulence.

2.4 The IMERSPEC Methodology

The algorithm of purposed methodology:

1) Solve the equation (16) in Fourier spectral space and obtain the temporal parameter $\hat{u}_l^*\left(\vec{k},t+\Delta t\right)$, using the low dispersion and low storage Runge-Kutta method proposed by [15];

2) Use the Inverse Fast Fourier Transformer in $\hat{u}_l^*\left(\vec{k},t+\Delta t\right)$ and obtain $u_l^*\left(\vec{x},t+\Delta t\right)$ at physic space in the domain Ω;

3) Interpolate $u_l^*\left(\vec{x},t+\Delta t\right)$ for the Lagrangean domain by equation (4), and obtain $u_l^*\left(\vec{x}_k,t+\Delta t\right)$;

4) Calculate the Lagrangean force, $F_l\left(\vec{x}_k,t+\Delta t\right)$, by equation (10).

5) Distribute the $F_l\left(\vec{x}_k,t+\Delta t\right)$ by equation (4), and obtain $f_l\left(\vec{x},t+\Delta t\right)$ in Eulerian domain;

6) Update the Eulerian velocity, $u_l\left(\vec{x},t+\Delta t\right)$ by equation (11) and transform to the spectral space obtaining $\hat{u}_l\left(\vec{k},t+\Delta t\right)$ and returned to step 1.

3 RESULTS

In order to validate the proposed methodology and the developed numerical code, three typical problems, normally, used in CFD were chosen. The first one is the a manufactured solution, which gives an analytic solution to incompressible two-dimensional Navier-Stokes equations, with periodic boundary conditions. This case was useful in order to verify the developed pseudo-spectral code without and with immersed boundary. The second one is the Poiseille flow, which has solid boundaries and an analytical solution. The third is the flow over a circular cylinder, which is a benchmark of CFD. This case shows the solution of incompressible two-dimensional Navier-Stokes equations using Fourier pseudo-spectral method with non-periodic boundary conditions imposed by an immersed boundary.

3.1 Manufactured solution without immersed boundary

The analytic equations to velocities component (u and v) and the pressure fields are given as a function of spatial coordinates (x and y) and time (t):

$$u(x,y,t) = U_\infty \sin(x)\cos(y)\cos(-2\pi\nu t), \tag{18}$$

$$\mathrm{v}(x,y,t) = -U_\infty \cos(x)\sin(y)\cos(-2\pi\nu t), \tag{19}$$

$$p(x,y,t) = 0.5U_\infty \left[\cos(x)^2 + \cos(y)^2\right]\cos(-2\pi\nu t)^2, \tag{20}$$

where U_∞ is the flow velocity amplitude in [*m/s*] and ν is the frequency [*1/s*].

From equations (18), (19) and (20) a source term is generated and added in equation (16). This way, it is possible to compare the analytical (u_a) and numerical (u_N) solutions. The L_2 norm of velocity error is adopted for this comparison:

$$L_2 = \sqrt{\frac{1}{N_x N_y}\sum_{i=1}^{N_x}\sum_{j=1}^{N_y}\left[u_N\left(x_i,y_j,t\right) - u_a\left(x_i,y_j,t\right)\right]^2} \tag{21}$$

We performs the simulations with a domain with $Lx=Ly=2\pi$ discretized with *32x32* collocation points. The time step used was given by *CFL=0.1* [1]. The result shown in Figure 2 is dimensionless by vortex diameter ($D=\pi$) and the maximal velocity (U_∞), thus $x^*=x/D$, $y^*=y/D$ and $p^*=p/(\rho U_\infty^2)$. The results of field pressure superposed by velocity vectors are displayed at Figure 2. It is possible to see the counter-rotating vortices.

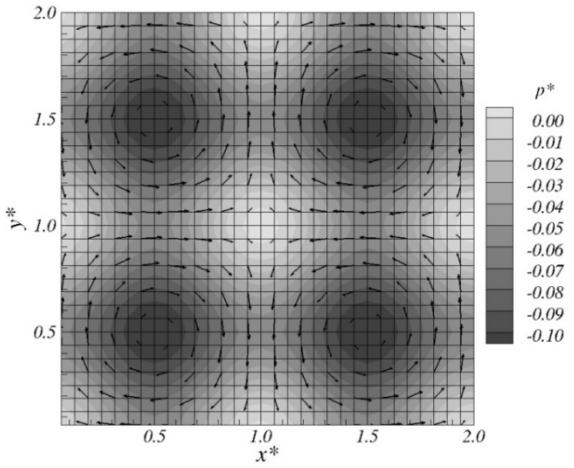

Figure 2: Pressure field superimposed by velocity vector at $t^*=1.0/\pi$.

The Figure 3 shows the temporal evolution of L_2 norm of horizontal velocity error, equation (21). The other velocity component and the pressure errors are the same magnitude. For the Fourier pseudo-spectral method the expected errors are the magnitude of round-off errors (for double precision is 10^{-16}) and this is confirmed by figure 3.

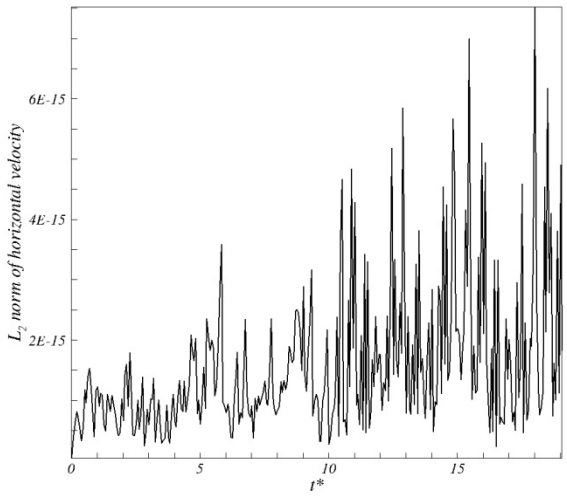

Figure 3: Temporal evolution of L_2 norm of horizontal velocity error.

3.2 Manufactured solution with immersed boundary

In order to verify the immersed boundary algorithm, the same simulations of [13] and [16] is performed. It is defined any geometry, which plays a role the immersed body in the flow. In the present case a circle with diameter $D^*=1$ is used, where D^* is the non-dimensional diameter and $D=\pi$ [m] is the reference length. Therefore, two domains are defined: Eulerian and Lagrangean, as can be seen in Figure 4, and the equations (18) and (19) are used in both domains.

Several different cases were simulated refining the grid mesh and was taken the L_2 norm of components velocities and pressure, comparing the analytical solution (u_a) and numerical solution (u_N). The grid spacing is Δx^*, the Reynolds number is $Re=10$, $U_\infty^* = 1.0$, $\rho=1,0$ [kg/m^3] the domain length is $Lx^*=Ly^*=2$ and the time step is defined by $CFL=0.01$. The immersed boundary velocity (U_{FI}) is defined by equations (15) and (16) in Lagrangean positions ($\vec{x}_k$) and at $t=t+dt$.

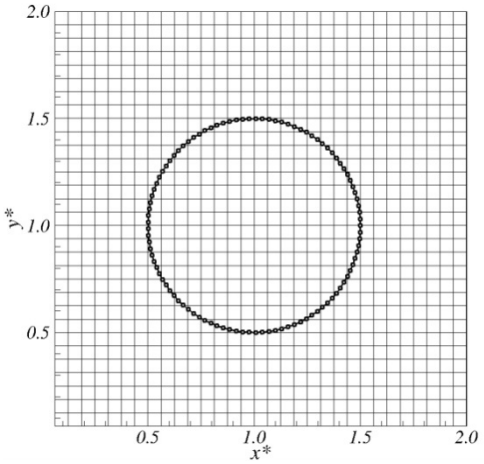

Figure 4: Sketch of Eulerian (Ω) and Lagrangean (Γ) domain.

The Figure 5 presents the comparison between L_2 norm as a function of grid refinement at time $t^*=1.0$. The results show decaying of the fourth order for all variables. It is a good result obtained using immersed boundary methodology.

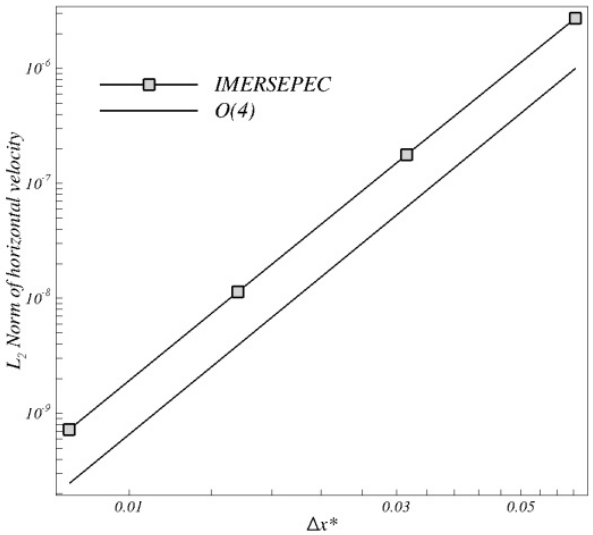

Figure 5: Comparison the L_2 norm as a function of mesh spacing.

3.3 Poiseuille Flow

The Poiseuille flow is other CFD problem used for codes verification, because it has an analytical solution [17]:

$$u_a(y) = C_1 y^2 + C_2 y + C_3, \tag{22}$$

where the coefficients C_1, C_2 and C_3 is done by:

$$C_1 = \frac{1}{2\mu}\frac{\Delta P}{L_x}, \tag{23}$$

$$C_2 = \frac{1}{D}\left[\left(u_{\max} - u_{\min}\right) - C_1\left(y_{\max}^2 - y_{\min}^2\right)\right], \tag{24}$$

$$C_3 = u_{\max} - C_1 y_{\max}^2 - \frac{1}{D}\left[\left(u_{\max} - u_{\min}\right) y_{\max} + C_1 y_{\max}\left(y_{\max}^2 - y_{\min}^2\right)\right]. \tag{25}$$

where y_{max} and y_{min} are the positions of superior and inferior walls, respectively; u_{max} and u_{min} is the velocity imposed at the walls. In the present simulations $u_{max}=u_{min}=0$ were used, D is the channel width and ΔP is pressure difference given by $\Delta P = p(x+\Delta x) - p(x)$. All dimensions and results fields are non-dimensionalized using as characteristic length the width channel $D = \pi\ [m]$ and characteristic mean velocity $U_\infty = 1.66\ [m/s]$.

The domain is show in Figure 6 (a). The channel is represented by immersed boundary (Γ_I), the domain flow of interests is Ω_I and the complementary domain (buffer domain) is Ω_B. In the present paper, we use the same procedure of manufactured solutions, with the force term replaced by a constant, which play the role of a pressure difference (ΔP). This procedure permits verify the accuracy of no-slip boundary conditions.

At the buffer domain (Ω_B) any pressure gradient can be imposed. We have used $\Delta P>0$, $\Delta P<0$ and $\Delta P=0$. In Ω_I $\Delta P<0$ is imposed, as can be seen in Figure 6 (b).

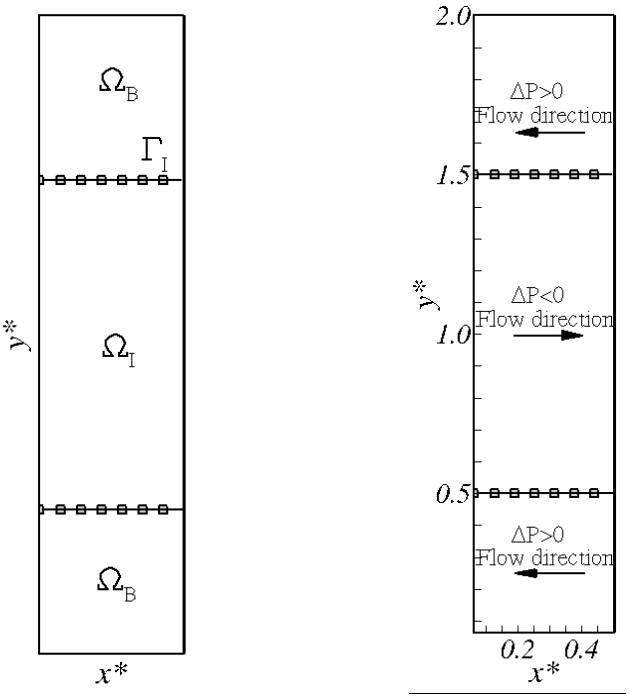

(a) (b)

Figure 6: a) The flow domain; b) Pressure difference and flow direction.

Simulations are performed in the domain $L_x^* = 0.5$ and $L_y^* = 2.0$, discretized with *Nx x Ny* collocation points. Walls positions is $y_{\min}^* = 0.5$ and $y_{\max}^* = 1.5$, time step is given by CFL=0.1 and the Reynolds number is *Re=100*, thus the viscosity is calculate by:

$$\nu = \frac{U_\infty D}{Re}. \tag{26}$$

The velocity profiles at $x^*=0.25$ in $t^*=50.0$ of differents ΔP in Ω_B are shows in Figure 7. A grid of $N_x=64$ and $N_y=256$ collocation points was used.

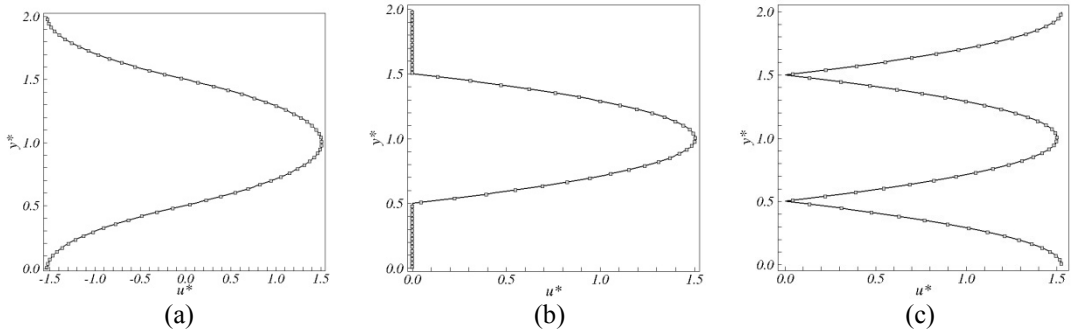

(a) (b) (c)

Figure 7: Velocity profiles at $x^*=0.25$ in $t^*=50.0$ for (a) $\Delta P>0$, (b) $\Delta P=0$ and (c) $\Delta P<0$ in Ω_B.

The differences of simulations are clear in Figure 8, which show the absolute velocity error between analytical and numerical solution for different grid refinement. For $\Delta P>0$ in buffer domain, the convergence rate reach second order. The maximal

order for this problem is limited by numerical solution that can be derivative only twice. For $\Delta P<0$ and $\Delta P=0$ the first order of convergence rate is obtained.

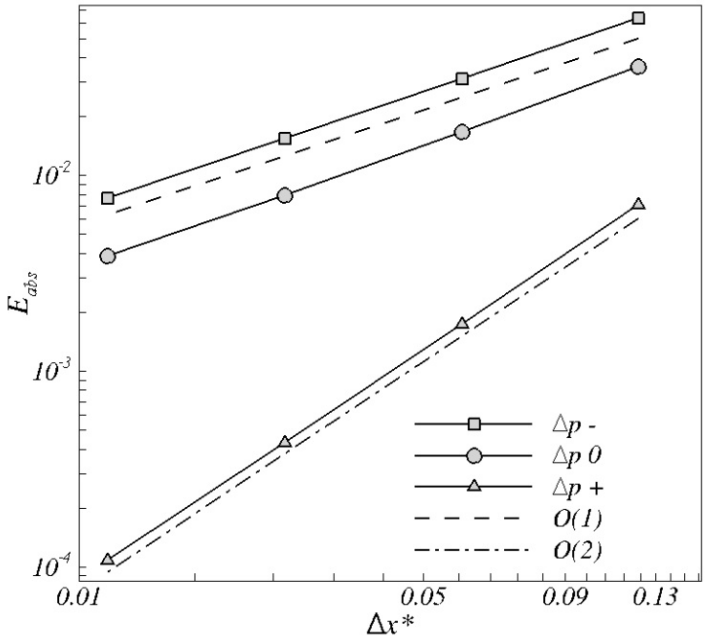

Figure 8: Convergence rate for different ΔP.

3.4 Flow over a cylinder

An inlet profile flow with velocity U_∞ in [*m/s*] is imposed. The flow cross the section of a circular cylinder, see Figure 9 and verify the drag and lift coefficients, equations (27) and (28), respectively. These variables determine the forces that act on bodies immersed in flow. The drag coefficient determines the resistance force of the fluid on the immersed body, while the lift coefficient determines the force that there is in perpendicular direction to incoming flow. Other parameter analyzed is the Strouhal number (*St*) which determines the non-dimensional vortex shedding frequency, equation (29).

$$Cd = \frac{-2\sum F_x}{\rho A_y U_\infty^2}, \tag{27}$$

$$Cl = \frac{-2\sum F_y}{\rho A_x U_\infty^2}, \tag{28}$$

$$St = \frac{fr \cdot D}{U_\infty}, \tag{29}$$

where: F_x and F_y are the forces calculated at each Lagrangean point with equation (7); A_x and A_y are the projected frontal area in direction x and y, respectively. In two-dimensional case these areas are given in [m^2] considered the axial dimension of surface equal to unity, D is the characteristic diameter and fr is the vortex shedding frequency downstream of cylinder.

The domain of all cases have been taken as 6π x 2π [m^2] and has been discretized with *384* x *128* collocation points. The cylinder has a diameter of $D=0,785$ [m], with *64* Lagrangean points. The cylinder position in domain is shown in Figure 9.

Periodicity conditions were used at the top and bottom boundary of the domain. The inflow condition is a uniform profile of velocity (U_∞=*1,0 m/s*), imposed by immersed boundary. A buffer zone was also used as [18]:

$$ZB = \phi\left(Q_l - Qt_l\right) \tag{30}$$

where Q is the problem solution, that is, u and v, Qt is the target solution, which required in the final buffer zone. In the present case, the target solution is an uniform profile U_∞, and ϕ is a parameter of stretching vortex, and it is calculated by equation (20):

$$\phi_\eta = \beta\left(\frac{x_\eta - x_{ZB}}{x_f - x_{ZB}}\right)^\alpha \tag{31}$$

where α=*3.0* and β=*1.0* [18], x_{ZB} and x_f give the length of the buffer zone, respectively, x_η is a generic position.

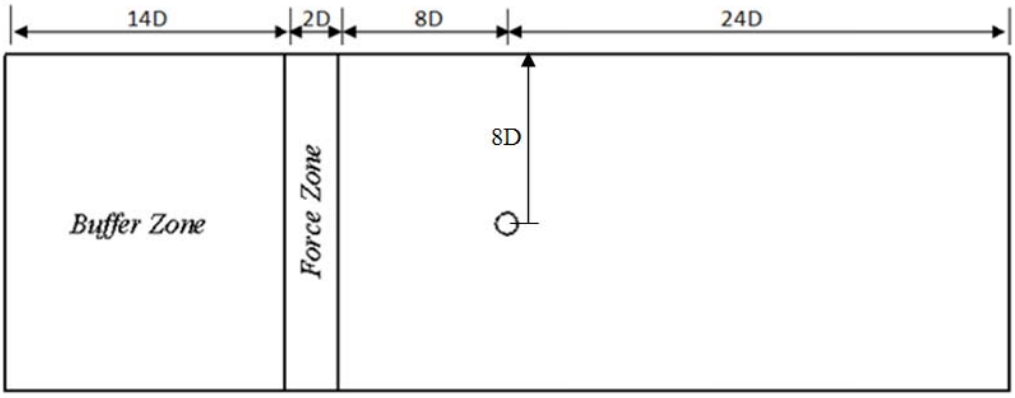

Figure 9: Calculus domain – circular cylinder.

The forcing zone or porous medium has a thickness of 2D, where is imposed the inflow profile by direct forcing, in order to have parallels streamlines.

Figure 10 shows vorticity field *(-1.0<w<1.0)* at time *t*=250*, for flow at *Re=100*. We can see the vortex shedding behind the cylinder, the influence of buffer and forcing zone. The eddy are damped at the buffer zone and are the forcing zone gives a parallel flow.

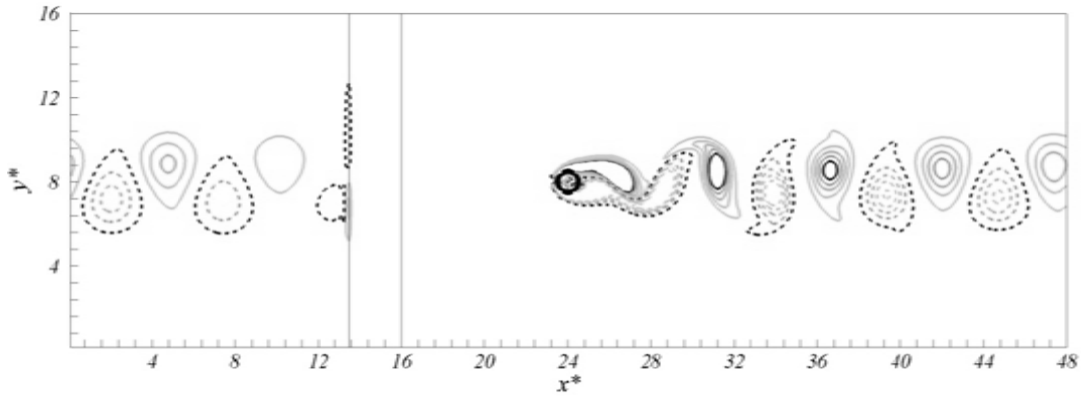

Figure 10: Isocontours of vorticity (*-1,0<w<1,0*) at *Re=100* in *t*=250*. - negative vortice; -- positive vorticity.

Figura 11 shows a zoom at the region of immersed object and velocity vectors. It is possible to see the flow deviation of the obstacle and the flow inside the boundary, which arise for close to divergence free.

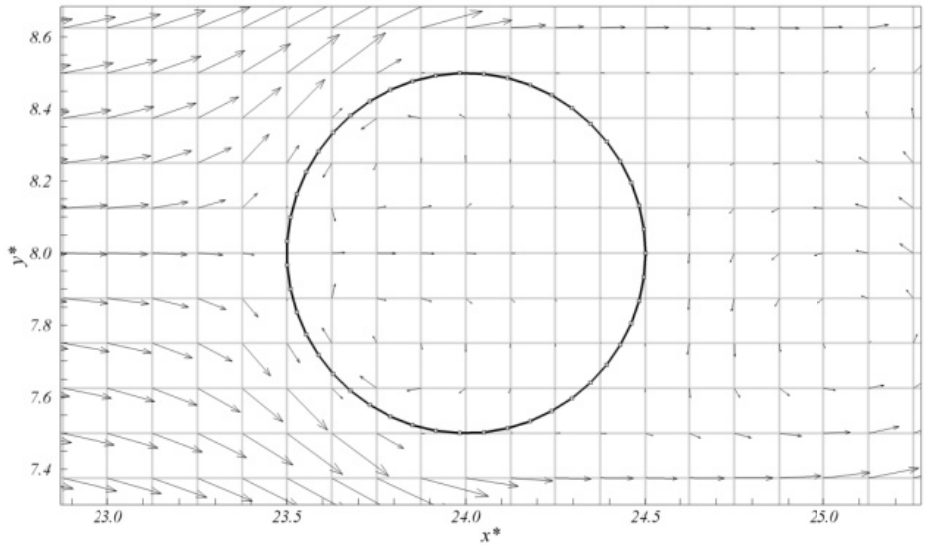

Figura 11: Velocity vectors at region of the immersed boundary.

The time evolution of vorticity field of simulation at *Re=100* is displayed at Figure 12.

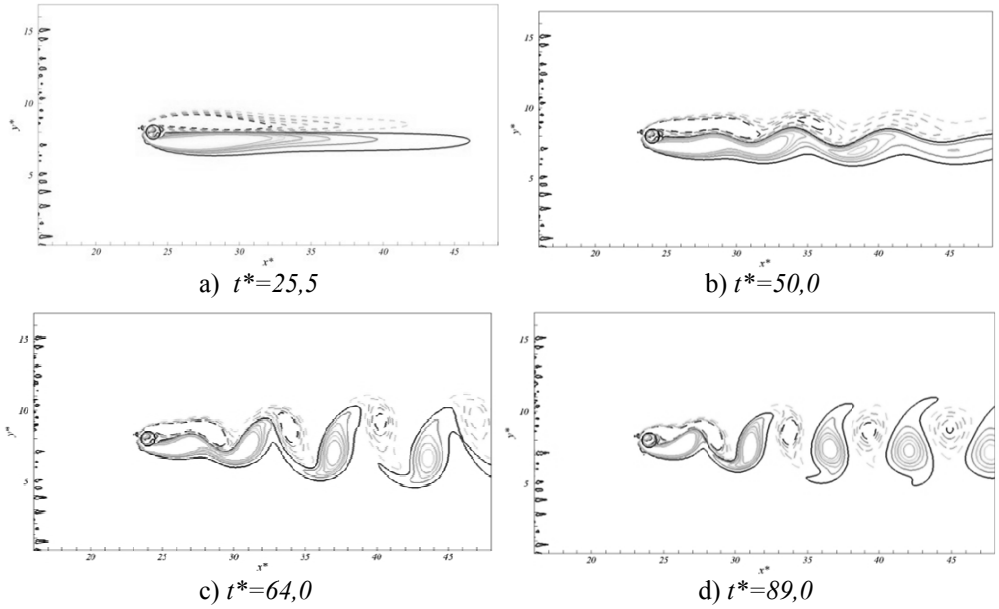

Figure 12: Temporal evolution of vorticity field at Re=100. -- negative vorticity; - positive vorticity.

Figure 12 (a) is the beginning of simulation, where we find two recirculation bubbles. In *t*=50*, Figure 12 (b), there is a formation of instability, and in the sequence appears the vortex shedding, *t*=64* and *t*=89*, Figure 12 (c) and (d) respectively.

In order to compare with other authors simulations of different Reynolds numbers is performed. Table 1 shows the comparison of *Cd*, *Cl* and *St*, equations (27), (28) and (29), respectively. The results of other authors [12], [19] and [20] were also used.

	[12]			[19]			[20]			[21]			Present work		
Re	*Cd*	*Cl*	*St*	*Cd*	*Cl*	*St*	*Cd*	*Cl*	*St*	*Cd*	*Cl*	*St*	*Cd*	*Cl*	*St*
100	1,39	0,20	0,160	1,44	0,33	0,165	1,42	0,34	0,171	1,39	0,34	0,160	1,45	0,35	0,175
150	1,37	0,25	0,175	1,47	0,58	0,184							1,37	0,49	0,200
200							1,42	0,66	0,202	1,38	0,68	0,192	1,27	0,47	0,213
300	1,22	0,27	0,190										1,08	0,39	0,221

Table 1: Comparison of drag coefficient and Strouhal number.

Figure 13 show the field of vorticity for different Reynolds numbers, Figure 13 (a), Re=45, for which we have two recirculating bubbles formed behind the cylinder. In Figure 13 (b), Re=60, the vortex shedding appear. Figure 13 (c), (d), (e) and (f) shows the influence of Reynolds number over a vortex shedding.

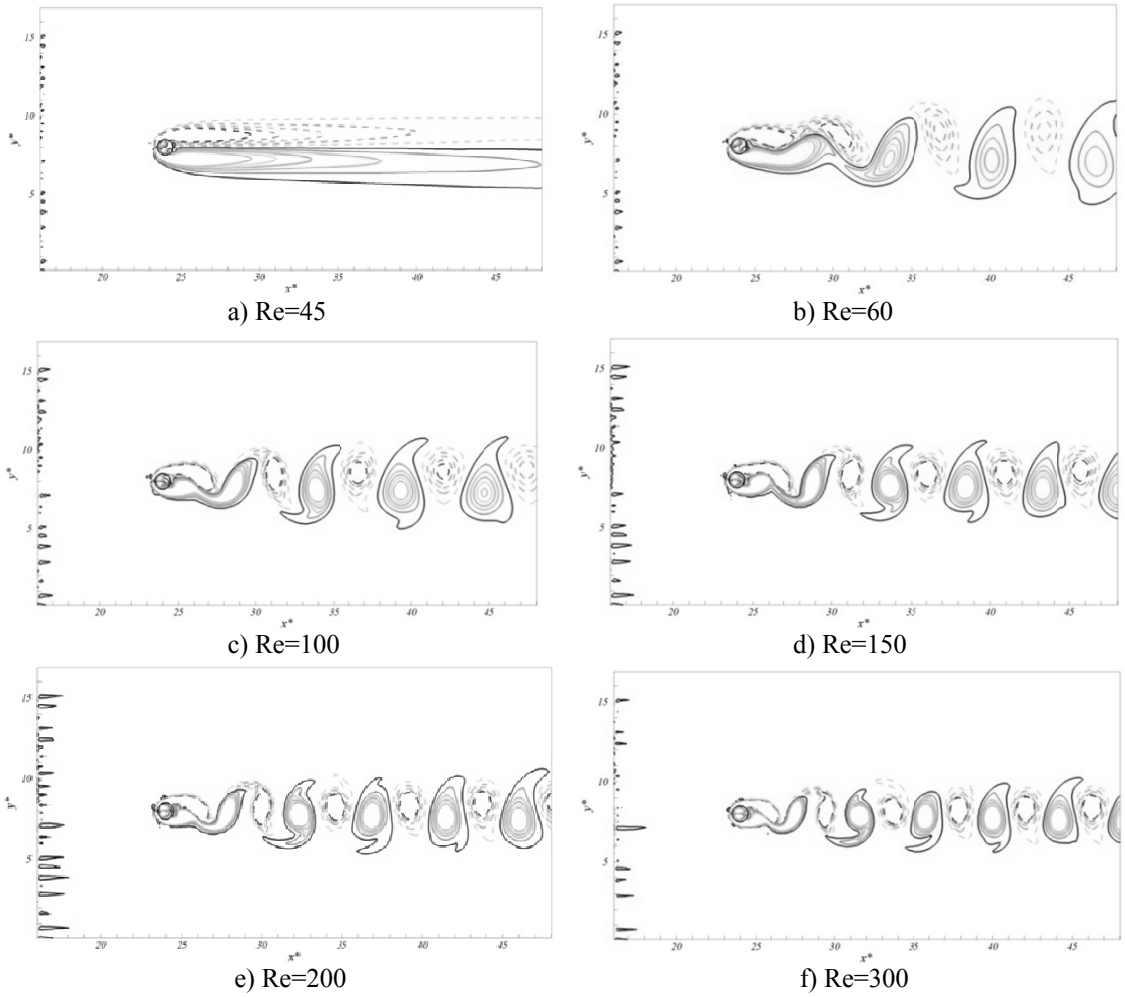

a) Re=45 b) Re=60

c) Re=100 d) Re=150

e) Re=200 f) Re=300

Figure 13: Isocontours of vorticity for different Reynolds numbers at $t^*=254$. -- negative vorticity; - positive vorticity.

Other important parameter of comparison is given by L_2 norm, equation (21), at the points of immersed boundary, which, rigorously, should be zero, but due to numeric approaches, is not exactly zero and depends on the Reynolds number, shown in Figure 14.

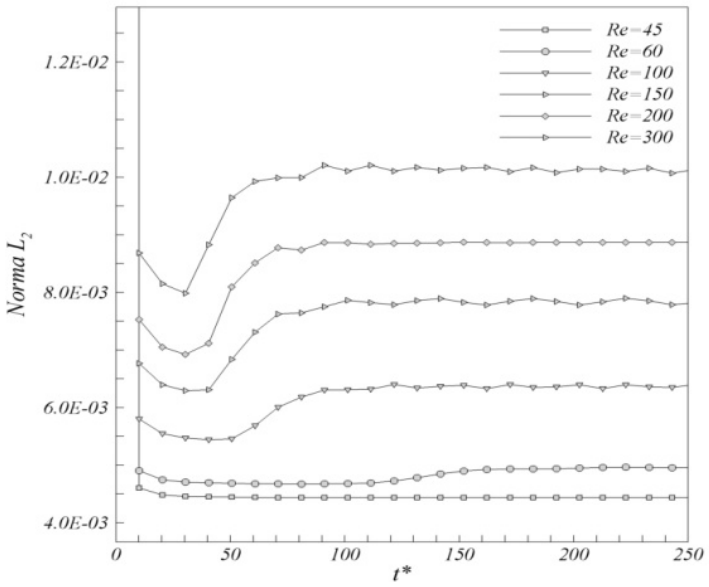

Figure 14: Temporal evolution of L_2 norm for different Reynolds numbers.

4 CONCLUSIONS

The present work shows the coupling between the pseudo-spectral method and immersed boundary method. Three features are highlighted:

- Pseudo-spectral algorithm is very efficient, because it do not need to solve the Poison equation for pressure field;
- Accuracy of Fourier pseudo-spectral method is high. It is demonstrated in simulations of manufacture solutions. Without immersed boundary we obtain round-off errors, and with immersed boundary we reach forth order of convergence;
- A buffer domain, as shown at section 3.4, is need for recover the inlet flow. Nevertheless, the algorithm is still efficient when compared with high order methods.

5 ACKNOWLEDGEMENTS

The authors thank the College of Engineering Mechanical (FEMEC) of the University Federal of the Uberlandia (UFU), Capes, FAPEMIG and CNPq for financial support.

REFERENCES

[1] J. H. Ferziger and M. Peric, Computational Methods for Fluid Dynamics, 1ft Edition, *Springer* (1996)

[2] S. Lele, Compact finite difference schemes with spectral-like resolution, *Journal of Computational Physics*. **103**, pp. 15–42 (1992)

[3] C. Canuto, M.Y. Hussaini, A. Quarteroni and T.A. Zang, Spectral methods: fundamentals in single domains, 1ft Edition, *Springer-Verlag* (2006).

[4] C. Canuto, M.Y. Hussaini, A. Quarteroni and T.A. Zang, Spectral methods: evolution to complex geometries and applications to fluid dynamics, 1ft Edition, *Springer-Verlag* (2007).

[5] J.B. Boyd, Chebyshev and Fourier spectral methods, 2nd Edition, *Dover Publications* (2000)

[6] T.W. Cooley, and J.W. Tukey, An algorithm for the machine calculation of complex Fourier series. *Mathematics Computation,* **19**, pp. 297-301 (1965)

[7] C.S. Peskin, Flow patterns around heart valves: a numerical method. *Journal of Computational Physics*, **10**, pp. 252-271 (1972)

[8] D. Goldstein, T. Adachi, and H. Sakata, Modeling a no-slip flow with an external force field. *Journal Computational Physics*. **105**, pp. 354 (1993)

[9] Z. Wang, J. Fan and K. Luo, Combined multi-direct forcing and immersed boundary method for simulating flows with moving particles. *International Journal of Multiphase Flow*. **34**, pp. 283-302 (2008)

[10] S. Enriquez-Remigio, and A. Silveira-Neto, A new modeling of fluid-structure interaction problems through immersed boundary method/virtual physical model (IBM/VPM), In proceedings of the CONGRESSO BRASILEIRO DE ENGENHEIRA MECÂNICA, COBEM 2007, Brasília (2007)

[11] B.E. Griffith and C.S. Peskin, On the order of accuracy of the immersed boundary method: Higher order convergence rates for sufficiently smooth problems. *Journal Computational Physics*. **208**, p. 75-105 (2005)

[12] A. Lima e Silva, A. Silveira-Neto, and J. Damasceno, Numerical simulation of two dimensional flows over a circular cylinder using the immersed boundary method. *Journal of Computational Physics*, **189**, pp. 351–370 (2003)

[13] M. Uhlmann, An immersed boundary method with direct forcing for the simulation of particulate flows. *Journal of Computational Physics*. **209**, pp. 448-476 (2005)

[14] W.L. Briggs and V.E. HENSON, The DFT. 1st Edition, **Vol. I,** *SIAM* (1995)

[15] J. BERLAND, C. BOGEY and C. BAILLY, Low-dissipation and low-dispersion fourth-order Runge–Kutta algorithm. *Computers & Fluids,* **35**, pp. 1459-1463 (2006)

[16] J. Kim, D. Kim and H. Choi, An immersed-boundary finite-volume method for simulations of flow in complex geometries. *Journal of Computational Physics*. **171**, pp. 132-150 (2001)

[17] R.W. Fox, A.T. McDonald and P.J. Pritchard, Introduction to Fluid Mechanics. 6th Edition, **Vol. I,** *LTC* (2006)

[18] A. Uzun, 3-D Large-eddy simulation for jet aeroacoustics. *Pardue University*, pp. 1-233 (2003)

[19] M.C. Lai and C.S. Peskin, An immersed boundary method with formal second order accuracy and reduced numerical viscosity. *Journal of Computational Physics*. **160**, pp. 705–719 (2000)

[20] S. Xu and Z.J. Wang, An immersed interface method for simulating the interaction of a fluid with moving boundaries. *Journal of Computational Physics.* **216**, pp. 454-493 (2006)

[21] D.V. Le, B.C. Khoo and K.M. Lim, An implicit-forcing immersed boundary method for simulating viscous flows in irregular domains. *Computer Methods in Applied Mechanics and Engineering*. **197**, pp. 2119-2130 (2008)